Physiologic Rate of Carrier-mediated Ca^{2+} Entry Matches Active Extrusion in Human Erythrocytes

SANJAY A. DESAI, PAUL H. SCHLESINGER, and DONALD J. KROGSTAD

From the Departments of Cell Biology, Biomedical Research, Medicine, Pathology, and Mechanical Engineering, Washington University, St. Louis, Missouri 63110

ABSTRACT The intracellular Ca^{2+} concentration of nearly all cells is kept at submicromolar levels. The magnitudes of transmembrane Ca^{2+} movement that maintain this steady state in the human red blood cell have long been debated. Although there is agreement that the physiologic extrusion of Ca^{2+} by the well-characterized Ca^{2+} ATPase amounts to 45 μmol/liter cells per h (1982. *Nature (Lond.)*. 298:478–481), the reported passive entry rates in physiological saline (2–20 μmol/liter cells per h) are all substantially lower. This discrepancy could be due to incomplete inhibition of the pump in the previous measurements of Ca^{2+} entry. We therefore examined both rate and mechanism of entry after completely inactivating the pump. This required pretreatment with iodoacetamide (to lower the intracellular ATP concentration) and vanadate (to inhibit any residual Ca^{2+} pump activity). The rate of Ca^{2+} entry (53 μmol/liter cells per h) was now found to be comparable to the accepted extrusion rate. Entry closely obeyed Michaelis-Menten kinetics (V_{max} = 321 ± 17 nmol Ca/g dry wt per h, K_m = 1.26 ± 0.13 mM), was competitively inhibited by external Sr^{2+} (K_i = 10.8 ± 1.2 mM), and was accelerated by intracellular Ca^{2+}. $^{45}Ca^{2+}$ efflux from these pump-inactivated cells was also accelerated by either external Ca^{2+} or Sr^{2+}. These accelerating effects of divalent cations on the opposite (*trans*) face of the membrane rule out a simple channel. Substrate-gated channels are also ruled out: cells equilibrated with $^{45}Ca^{2+}$ lost the isotope when unlabeled Ca^{2+} or Sr^{2+} was added externally. Thus, passive Ca^{2+} movements occur predominantly by a reversible carrier-mediated mechanism for which Sr^{2+} is an alternate substrate. The carrier's intrinsic affinity constants for Ca^{2+} and Sr^{2+}, 1.46 and 0.37 mM^{-1}, respectively, indicate that Ca^{2+} is the preferred substrate.

INTRODUCTION

Fluctuations in the free intracellular Ca^{2+} concentration, $[Ca^{2+}]_i$, are thought to trigger many cellular processes by activating Ca^{2+}-dependent enzymes such as protein kinase C, actin-myosin ATPase, or the Ca^{2+}-dependent K^+ channel. Steady-state $[Ca^{2+}]_i$ is largely determined by the balance between the active extrusion and passive entry mechanisms present in the plasma membrane of most cells (Schatz-

Address reprint requests to Dr. Donald Krogstad, Department of Pathology, Box 8118, Washington University School of Medicine, 660 S. Euclid Ave., St. Louis, MO 63110.

J. GEN. PHYSIOL. © The Rockefeller University Press · 0022-1295/91/08/0349/16 $2.00
Volume 98 August 1991 349–364

mann, 1985). Despite the fundamental regulatory role of $[Ca^{2+}]_i$, previously reported Ca^{2+} entry and exit rates have not matched quantitatively under physiologic conditions.

In the red blood cell (RBC), active extrusion is mediated by an efficient Ca^{2+} ATPase pump. This pump has been studied carefully (see Schatzmann, 1985, and Carafoli, 1987, for reviews); its high affinity for intracellular Ca^{2+} maintains a steady-state $[Ca^{2+}]_i$ of 20–30 nM (Lew et al., 1982), a value some 50,000-fold lower than the external free Ca^{2+} concentration, $[Ca^{2+}]_o$.

In contrast, the downhill entry of Ca^{2+} is poorly understood. $^{45}Ca^{2+}$ tracer fluxes reveal it only when the Ca^{2+} pump is inhibited. While there are no complete and specific Ca^{2+} pump inhibitors, several approaches—La^{3+} blockade, ATP or Mg^{2+} depletion (Ferreira and Lew, 1977; McNamara and Wiley, 1986), vanadate pretreatment (Varecka and Carafoli, 1982; Varecka et al., 1986), and Ca^{2+} chelator loading (Lew et al., 1982; Tiffert et al., 1984)—have been used to study passive entry either by slowing the Ca^{2+} pump or by lowering $[Ca^{2+}]_i$. With these various methods, diverse entry rates in physiological saline, 2–20 μmol/liter cells per h, have been reported, all substantially lower than the accepted rate of active extrusion, 45 μmol/liter cells per h (Lew et al., 1982). Both the diversity of entry rates and the apparent imbalance between entry and exit are consistent with incomplete levels of pump inhibition in these previous studies.

This paper examines the passive movement of Ca^{2+} across the human RBC membrane under conditions that completely inactivate the Ca^{2+} extrusion pump. Under these conditions, passive Ca^{2+} movement is mediated almost exclusively by a reversible carrier which also transports Sr^{2+}. Our kinetic analysis indicates that this carrier mediates the entry of Ca^{2+} without exchange for intracellular cations under physiologic conditions. This influx also matches the rate of active extrusion by the Ca^{2+} pump, thus maintaining a steady state $[Ca^{2+}]_i$.

MATERIALS AND METHODS

Preparation and Storage of RBCs

Human blood was drawn into CPD (citrate, phosphate, dextrose—an anticoagulant) and centrifuged at 1,500 *g* in a Sorvall GLC-2B centrifuge. The plasma was removed and the cells were stored at a hematocrit (Hct) of 70% in ADSOL (a preservative) at 4°C for up to 3 wk under sterile conditions. The rates of passive $^{45}Ca^{2+}$ movement did not change during this storage period.

Frequently Used Media

Several frequently used media have been assigned the following abbreviations:

Medium A: 130 mM KCl, 30 mM sucrose, 20 mM HEPES, pH adjusted to 7.4 with 5 N KOH.

Medium B: 80 mM KCl, 60 mM NaCl, 20 mM HEPES, pH adjusted to 7.4 with 5 N KOH.

Medium C: 130 mM KCl, 30 mM sucrose, 20 mM HEPES, 5 mM Na_3VO_4, 20 μM valinomycin, pH adjusted to 7.4 with 5 N KOH or 1 N HCl as required.

Reagents

Benz 2 (MAPTAM) was purchased from Calbiochem Corp. (La Jolla, CA). $^{45}CaCl_2$ and $^{90}Sr(NO_3)_2$ were obtained from Amersham Corp. (Arlington Heights, IL). All other reagents were of analytical grade and were obtained from Sigma Chemical Co. (St. Louis, MO).

Ca^{2+} Pump Inactivation

RBCs were washed and the buffy coats were removed before ATP depletion with 6 mM iodoacetamide (a glycolytic inhibitor), 10 mM inosine (Lew, 1971), and 0.1 mM EGTA at 5% Hct and 37°C for 3 h (Ferreira and Lew, 1977). To produce as low an $[ATP]_i$ as possible, two steps were taken to maximize the consumption of ATP during this incubation with iodoacetamide. First, ATP depletion was carried out in medium A, which contained 130 mM K^+, to facilitate ATP consumption by the Na^+/K^+ pump. Second, the ATPase inhibitor, vanadate, was added only after the incubation with iodoacetamide.

Vanadate (Bond and Hudgins, 1978; Niggli et al., 1981) was used to inhibit Ca^{2+} pump activity remaining after ATP depletion. Preincubation with vanadate lasted at least 30 min to ensure its entry by the anion exchanger, a process with a $t_{1/2}$ of 4 min (Cantley et al., 1978).

Ca^{2+} Chelator Loading

To measure zero *trans* influx rates, RBCs were loaded with the Ca^{2+} chelator Benz 2 (Tsien, 1981) by adding 0.1 mM of the chelator's acetoxymethyl tetraester (250 mM stock solution in DMSO) to the ATP depletion medium.

Ca^{2+} Loading

Two methods were used to load cells with Ca^{2+}. To load $^{45}Ca^{2+}$ concentrations ≤ 0.4 mM for efflux studies, ATP-depleted cells were incubated with 1 or 2 mM $[^{45}Ca^{2+}]_o$ at 5% Hct and 35°C with continuous stirring for up to 50 h under sterile conditions. When a higher $[Ca^{2+}]_i$ was desired, 0.1 μM A23187, a Ca^{2+} ionophore, was used with 4 mM $[Ca^{2+}]_o$ (see legend of Fig. 3 *A* for details).

Measurement of RBC $^{45}Ca^{2+}$ Content

RBC $^{45}Ca^{2+}$ flux was terminated by three to four rapid washes in ice-cold medium A with 1 mM EGTA (which required ~2 min) and centrifugation through a 4:1 silicone/mineral oil mixture at 11,000 *g* for 10 s. The pellet was then digested in a 1:2 Protosol® (tissue solubilizer)/ethanol mixture, decolorized with 30% H_2O_2, and neutralized with 1 N HCl before β-counting in 8 ml of Universol® scintillation cocktail.

Establishment and Determination of a Donnan Membrane Potential

A constant, known V_m (membrane potential) was required to rule out kinetic artifacts due to a changing V_m and to calculate the carrier's intrinsic affinity constants for Ca^{2+} and Sr^{2+}. To establish Donnan equilibrium, ATP-depleted RBCs were incubated in medium C (which contained 20 μM valinomycin, a K^+ ionophore) for 7 h before $^{45}Ca^{2+}$ flux measurements. To estimate the Donnan V_m, these cells were packed in a 400-μl microfuge tube by centrifugation at 11,000 *g* for 15 min and collected after cutting the tube below the cell–saline interface (extracellular trapping 1.5% by volume using $^{45}Ca^{2+}$-EGTA). After weighing, the cells were lysed in 1,000 vol of distilled H_2O to determine their intracellular K^+ content with a model 251 atomic absorption spectrophotometer (Instrumentation Laboratory, Inc., Lexington, MA). K^+

standards were prepared in the same distilled H_2O. The K^+ content was converted to an intracellular K^+ concentration using the percent cell H_2O by weight, which was determined using equivalent samples weighed before and after drying to constant weight at 70°C. V_m, calculated using the Nernst equation for K^+, reached a steady-state value of −4 mV, in good agreement with the predicted Donnan V_m of −7 mV for medium C (Freedman and Hoffman, 1979).

Units of Flux Measurements

Rates of transport are reported in nanomoles per gram dry weight per hour, rather than micromoles per liter cells per hour, because the former is readily converted to rates per RBC (grams dried cell solids = 3.1×10^{10} RBCs) without correcting for variations in cell volume (Weith et al., 1974). In each experiment, an equivalent sample of RBCs, taken immediately before the flux measurement, was dried as above and used to calibrate the measured rates. Hemolysis during the 1 h required to measure entry rates (Fig. 2) was <2% (determined by weighing RBC samples collected after the flux measurements) and was ignored.

RESULTS

Complete Inactivation of the Ca^{2+} Pump

After pretreatment with 6 mM iodoacetamide, 0.5 mM vanadate was required to block residual Ca^{2+} pump activity. Higher vanadate concentrations had no further effect on the $^{45}Ca^{2+}$ efflux rate. Thus, the Ca^{2+} pump was completely inactivated (legend, Fig. 1 *A*) and any remaining $^{45}Ca^{2+}$ efflux was passive.

Unidirectional Passive Influx

The unidirectional influx rate could now be measured by adding extracellular $^{45}Ca^{2+}$ after the cells were loaded with the Ca^{2+} chelator Benz 2. In cells not so loaded (Fig. 1 *B, filled circles*) the rate of accumulation decreased gradually, mainly because of increasing passive $^{45}Ca^{2+}$ efflux. In Benz 2–loaded cells, the intracellular chelator allowed a constant rate of $^{45}Ca^{2+}$ accumulation for ~2 h (Fig. 1 *B, filled triangles*). The identical initial influx rates with or without Benz 2 indicate that the chelator does not affect RBC Ca^{2+} permeability.

The omission of vanadate produced substantially lower influx (Fig. 1 *B, open symbols*). Thus, even after ATP depletion and Benz 2–loading, vanadate was required to inhibit residual Ca^{2+} pumping. Indeed, these data demonstrate why previously reported entry rates (measured after either ATP depletion or exposure to vanadate, but not both) were two- to threefold lower than required to match physiologic Ca^{2+} pumping.

At $[Ca^{2+}]_o < 5$ mM, influx obeys Michaelis-Menten kinetics, suggesting a saturable process and the translocation of one Ca^{2+} ion per reaction cycle. At higher $[Ca^{2+}]_o$ (5–30 mM), a nonsaturating component becomes apparent (Fig. 2). The unidirectional $^{45}Ca^{2+}$ influx rates (v), observed at different Ca_o, were fitted with:

$$v = \frac{V_{max} \times Ca_o}{K_m + Ca_o} + L \times Ca_o \quad (1)$$

using the nonlinear, weighted, least-squares method (De Weer and Lowe, 1973).

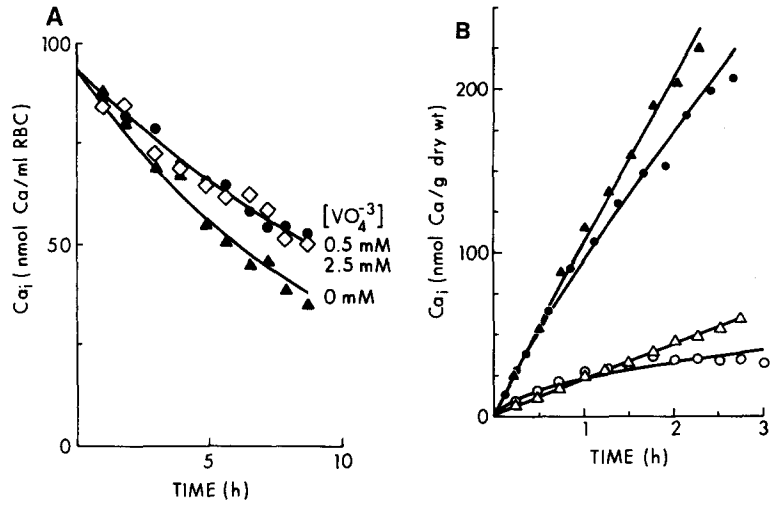

FIGURE 1. Unidirectional passive Ca^{2+} transport. (*A*) Effect of vanadate on Ca^{2+} efflux from ATP-depleted RBCs. ATP-depleted, $^{45}Ca^{2+}$-loaded RBCs were washed and resuspended at 37°C and 0.2% Hct in medium B with 1 mM EGTA and 0 mM (*triangles*), 0.5 mM (*circles*), or 2.5 mM (*diamonds*) Na_3VO_4 at pH 7.4. Solid lines in this figure and in Figs. 1 *B*, 3, *A* and *B*, 4 *C*, and 7 represent least-squares fits of single exponentials. Notice that increasing the $[VO_4^{-3}]$ fivefold (from 0.5 to 2.5 mM) had no further effect on the rate of $^{45}Ca^{2+}$ efflux. (*B*) Effect of Benz 2 on passive Ca^{2+} accumulation. ATP-depleted RBCs with (*triangles*) or without (*circles*) Benz 2 loading were incubated in medium A with 2.5 mM Na_3VO_4 at pH 7.4 for 2 h (*filled symbols*). To measure $^{45}Ca^{2+}$ accumulation (0.5 mM $^{45}CaCl_2$), these RBCs were incubated at 20% Hct and 37°C in medium A with (*filled symbols*) or without (*open symbols*) 2.5 mM Na_3VO_4 (pH 7.4). $[VO_4^{-3}]$ greater than 2.5 mM did not further increase influx, indicating that the Ca^{2+} pump was completely inactivated (not shown).

Estimates of the parameters and their standard errors were V_{max} = 291 ± 18 nmol Ca/g dry wt per h, K_m = 1.10 ± 0.12 mM, and L = 13.94 ± 1.00 nmol Ca/(g dry wt per h per mM). To achieve a constant residual variance over the range of $[Ca^{2+}]_o$, the data were weighted by $1/v^2$ in the least-squares algorithm. This weighting did not

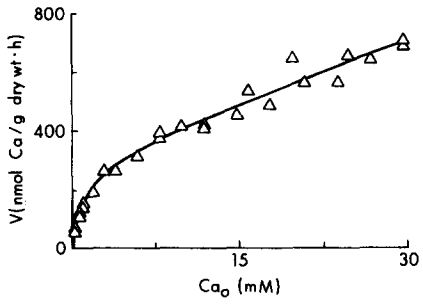

FIGURE 2. Unidirectional passive $^{45}Ca^{2+}$ influx rates at various Ca_o. ATP-depleted, Benz 2–loaded RBCs were preincubated in medium C for 7 h at 37°C before measuring influx rates in the same medium with $^{45}CaCl_2$. Solid line is the best fit to Eq. 1. Medium C contained negligible contaminant Ca^{2+} (<5 μM by atomic absorption) and its nominal $[Ca^{2+}]_o$ was not altered by adding RBCs, ruling out artifactual causes for the nonlinear flux concentration profiles. These rates were unchanged when valinomycin was omitted or when the vanadate concentration was raised from 5 to 10 mM. Thus, these agents do not alter RBC Ca^{2+} permeability.

significantly alter parameter estimates, but was required to satisfy the constant variance assumption used to estimate standard errors (Draper and Smith, 1981).

For physiologic $[Ca^{2+}]_o$ (1.3 mM) influx is 176 nmol/g dry wt per h or 53 μmol/liter cells per h, in good agreement with the known physiologic Ca^{2+} pump rate of 45 μmol/liter cells per h (Lew et al., 1982). Replacement of KCl by NaCl produced no changes in $^{45}Ca^{2+}$ influx or efflux rates and thus ruled out a Na^+/Ca^{2+} exchanger (data not shown).

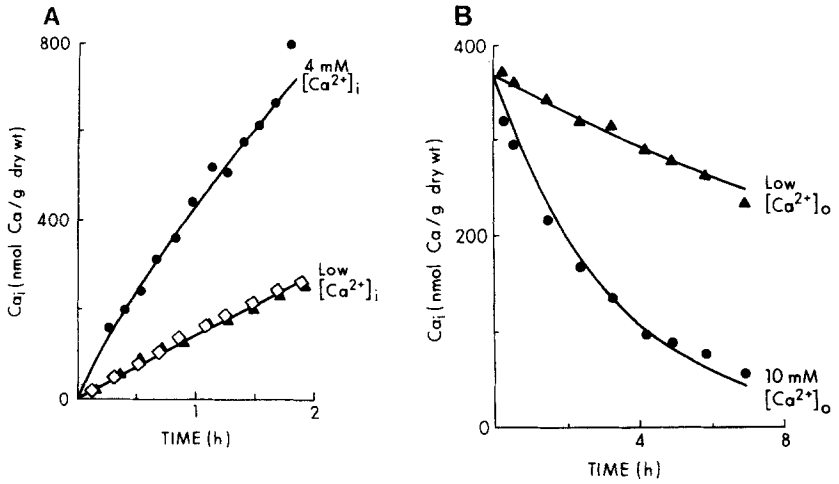

FIGURE 3. *Trans* acceleration. (*A*) Effect of *Trans* Ca^{2+} on passive $^{45}Ca^{2+}$ influx. After ATP depletion without Benz 2 loading, RBCs were incubated at 5% Hct and 37°C for 18 h in medium C (*triangles*), in medium C with 0.1 μM A23187 and 0.1 mM EGTA (*diamonds*), or in medium C with 0.1 μM A23187 and 4 mM unlabeled $CaCl_2$ (*circles*). RBCs exposed to A23187 were then washed five times at a Hct of 5% in medium A with 50 μM BSA at pH 7.4. After three additional washes in medium C, $^{45}Ca^{2+}$ accumulation was measured in medium C with 1 mM $^{45}Ca^{2+}$. The ionophore concentration used was sufficient to load 4 mM unlabeled Ca^{2+} into RBCs, yet low enough that five BSA washes (Simonsen, 1980) restored the original Ca^{2+} permeability of the cells (compare diamonds and triangles). (*B*) Effect of *Trans* Ca^{2+} on passive Ca^{2+} efflux. The time course of $^{45}Ca^{2+}$ efflux from ATP-depleted, $^{45}Ca^{2+}$-loaded RBCs was followed in medium C with either 0.1 mM EGTA (*triangles*) or 10 mM $CaCl_2$ (*circles*).

Effects of Trans Unlabeled Ca^{2+}

To distinguish between the two simplest kinetic models for passive transport that obey Michaelis-Menten kinetics, the channel and carrier models (Stein, 1986), influx and efflux of $^{45}Ca^{2+}$ were examined with and without unlabeled Ca^{2+} on the *trans* side. Influx was studied in cells loaded with millimolar Ca^{2+} by incubation with 4 mM $[Ca^{2+}]_o$ and the Ca^{2+} ionophore A23187. After washing the cells with BSA to remove all detectable ionophore activity, $^{45}Ca^{2+}$ influx into these cells was threefold that into cells not loaded with Ca^{2+} (Fig. 3 *A*, legend). Similarly, efflux from cells loaded with

$^{45}Ca^{2+}$ was accelerated by raising external Ca^{2+} from low nanomolar levels (with 0.1 mM EGTA) to 10 mM (Fig. 3 *B*). These *trans* accelerations are incompatible with a simple channel and favor a carrier model (Lieb, 1982).

Effects of Cis and Trans Sr^{2+} on the Proposed Ca^{2+} Carrier

Sr^{2+} added to the extracellular medium competitively inhibited Ca^{2+} influx (Fig. 4, *A* [*inset*] and *B*). For Sr^{2+} concentrations up to 22.5 mM, the rate of $^{45}Ca^{2+}$ entry is given by:

$$v = \frac{V_{max} \times Ca_o}{K_m(1 + Sr_o/K_i) + Ca_o} + L \times Ca_o \quad (2)$$

(The second term represents the nonsaturating component described above.) The data fitted with this equation by the nonlinear, weighted, least-squares method yielded values for V_{max} of 321 ± 17 nmol Ca/g dry wt per h, for K_m of 1.26 ± 0.13 mM Ca_o, for K_i of 10.8 ± 1.2 mM Sr_o, and for L of 11.4 ± 0.9 nmol Ca/(g dry wt/h per mM) (Fig. 4 *A*). These estimates of V_{max} and K_m agree well with those obtained without Sr^{2+} (Fig. 2), verifying that simple competitive inhibition adequately describes the effect of external Sr^{2+} and that the Ca^{2+} carrier also binds Sr^{2+}.

If the carrier could bind but not translocate Sr^{2+}, *trans* Sr^{2+} would inhibit $^{45}Ca^{2+}$ flux; if, instead, Sr^{2+} were also translocated, acceleration by *trans* Sr^{2+} might be seen. Our data indicate that Sr^{2+} is transported: *trans* Sr^{2+} accelerated $^{45}Ca^{2+}$ efflux markedly (Fig. 4 *C*). We could not test for the acceleration of $^{45}Ca^{2+}$ influx by *trans* Sr^{2+} because we were unable to prepare cells loaded with millimolar Sr^{2+} (determined using $^{90}Sr^{2+}$; not shown).

Testing a Substrate-gated Channel Model

The observed acceleration of passive $^{45}Ca^{2+}$ transport by *trans* Ca^{2+} and *trans* Sr^{2+} (Figs. 3, *A* and *B*, and 4 *C*) suggests a simple carrier which presents its binding site to one side of the membrane at a time (Lieb, 1982). Although a simple channel can exhibit only *trans* inhibition (Läuger, 1980) and is thus incompatible with our observations, a channel gated by Ca^{2+} and Sr^{2+} could in principle exhibit *trans* acceleration. Such a channel would require positive gating by *trans* Ca^{2+} and Sr^{2+} in both directions as well as competitive inhibition by *cis* Sr^{2+}. These are complicated constraints indeed. To distinguish unambiguously between the substrate-gated channel and simple carrier models, we added external unlabeled Ca^{2+} or Sr^{2+} to cells in which $^{45}Ca^{2+}$ was at electrochemical equilibrium. Added substrate might increase the permeability of a gated channel, but cannot provide the energy to drive label away from equilibrium because label and added substrates move independently (Fig. 5, *dashed line*). For a simple carrier, however, labeled and unlabeled substrates do not move independently. The imposed inward gradient of unlabeled substrate could drive label out by countertransport. In our experiment the cells in fact lost $^{45}Ca^{2+}$, confirming the simple carrier model and ruling out a substrate-gated channel (Fig. 5).

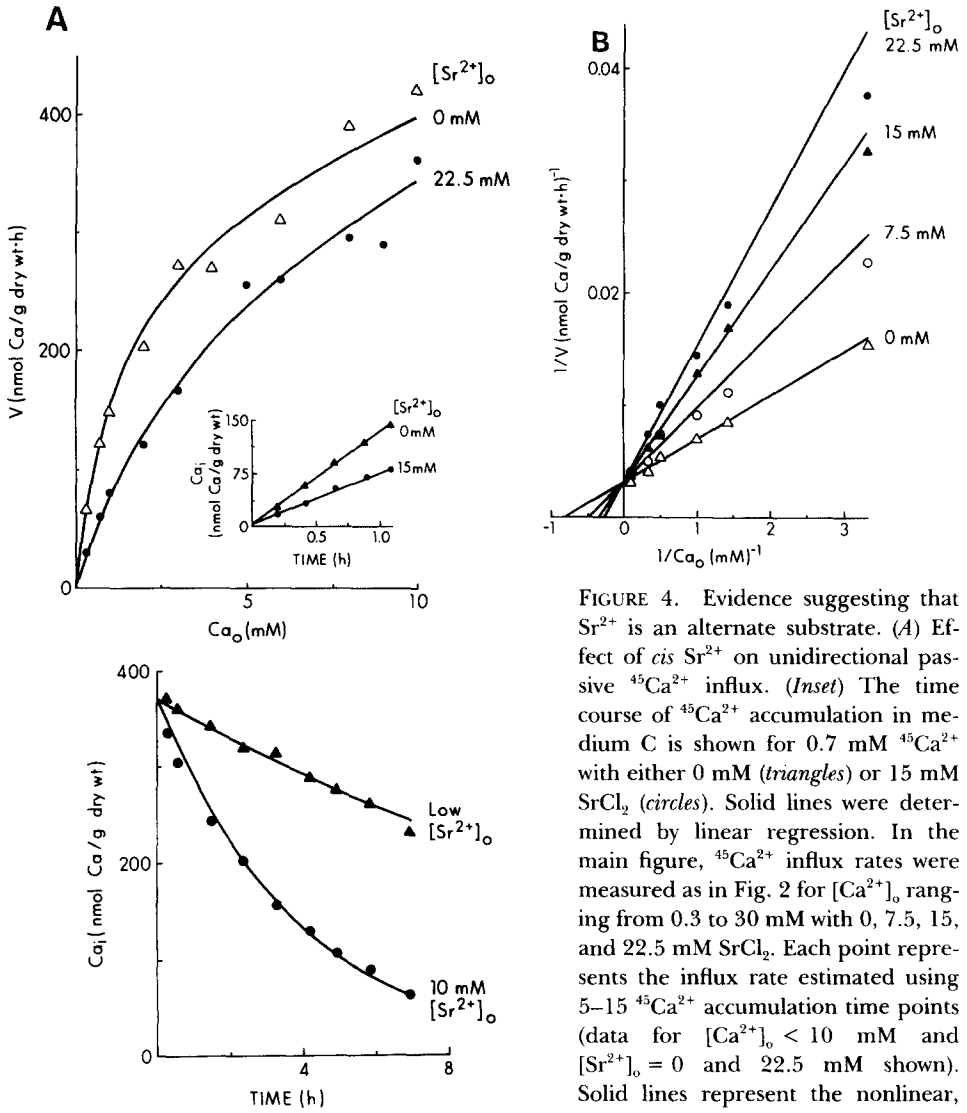

FIGURE 4. Evidence suggesting that Sr^{2+} is an alternate substrate. (*A*) Effect of *cis* Sr^{2+} on unidirectional passive $^{45}Ca^{2+}$ influx. (*Inset*) The time course of $^{45}Ca^{2+}$ accumulation in medium C is shown for 0.7 mM $^{45}Ca^{2+}$ with either 0 mM (*triangles*) or 15 mM $SrCl_2$ (*circles*). Solid lines were determined by linear regression. In the main figure, $^{45}Ca^{2+}$ influx rates were measured as in Fig. 2 for $[Ca^{2+}]_o$ ranging from 0.3 to 30 mM with 0, 7.5, 15, and 22.5 mM $SrCl_2$. Each point represents the influx rate estimated using 5–15 $^{45}Ca^{2+}$ accumulation time points (data for $[Ca^{2+}]_o < 10$ mM and $[Sr^{2+}]_o = 0$ and 22.5 mM shown). Solid lines represent the nonlinear, weighted, least-squares fit to Eq. 2. Examination of weighted residuals revealed that the fit was equally good for all $[Ca^{2+}]_o$ and $[Sr^{2+}]_o$. (*B*) Effect of *cis* Sr^{2+} on passive $^{45}Ca^{2+}$ influx: Lineweaver-Burk plot. The data described in the main figure of *A* are replotted on a Lineweaver-Burk plot after correction for nonsaturating uptake by subtracting $L \times Ca_o$ (L = 11.4 nmol Ca/[g dry wt/h per mM]). The solid lines represent the expected values calculated using the best estimates of K_m, V_{max}, and K_i by Sr^{2+} determined in Fig. 4 *A* (values listed in the text). A slightly better fit was obtained if Sr^{2+} inhibition of the nonsaturating component (~20% at the highest $[Sr^{2+}]_o$) was permitted (not shown here). (*C*) Effect of *trans* Sr^{2+} on passive $^{45}Ca^{2+}$ efflux. $^{45}Ca^{2+}$ efflux was followed in medium C with either 0.1 mM EGTA (*triangles;* same data as in Fig. 3 *B*) or 10 mM $SrCl_2$ (*circles*).

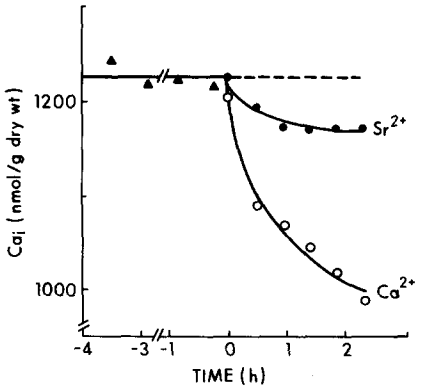

FIGURE 5. Effect of external unlabeled Ca^{2+} or Sr^{2+} on $^{45}Ca^{2+}$ equilibrium distribution. ATP-depleted RBCs were loaded with $^{45}Ca^{2+}$ by incubation in medium C with 1.0 mM $^{45}CaCl_2$ at 35°C for 39 h with continuous stirring, then washed and resuspended in medium C with 0.18 mM $^{45}CaCl_2$ (at the same specific activity) at 37°C for 12 h to demonstrate that the $^{45}Ca^{2+}$ content of the cells had come to equilibrium (*triangles*). At t = 0, 0.8 mM unlabeled $CaCl_2$ (*open circles*) or 0.8 mM $SrCl_2$ (*filled circles*) was added without significant dilution. The observed subsequent decrease in $^{45}Ca^{2+}$ content rules out substrate-gated channels, for which no change is expected (*dashed line*). Although this decrease should be transient, recovery could not be demonstrated because hemolysis did not permit quantitative measurements beyond 5 h. Before the addition of $CaCl_2$ or $SrCl_2$, intracellular free $^{45}Ca^{2+}$ was calculated to be 0.24 mM based on a membrane potential of −4 mV.

Our kinetic findings are most conservatively explained by a simple carrier with two charged substrates, Ca^{2+} and Sr^{2+}:

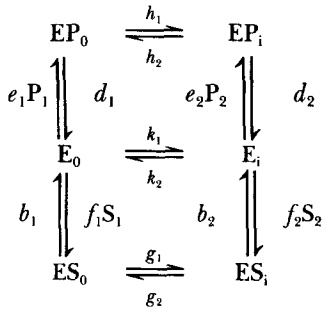

Scheme 1

In this scheme, E (enzyme) represents the unbound carrier, while ES and EP represent the carrier bound to substrates S or P, which stand for Ca^{2+} and Sr^{2+}, respectively. Subscripts o and i refer to the outward- and inward-facing carrier intermediates. Lowercase letters represent first-order rate constants for each of the 14 allowed reactions (*arrows*). Pseudo-first-order rate constants (rate constants multiplied by appropriate free substrate concentrations) are also indicated. Slippage, the interconversion of E_o and E_i without Ca^{2+} or Sr^{2+} transport, is necessary to explain the $^{45}Ca^{2+}$ fluxes observed without *trans* substrate (e.g., efflux into EGTA-containing solutions [Fig. 1 *A*] or influx into Benz 2–loaded cells [Fig. 1 *B*]).

The unidirectional influx and efflux rates, v_{in} and v_{ef}, for the carrier in Scheme 1, derived using the method described in Stein (1986), are given by Eqs. A1 and A2 in the Appendix. These equations are of the most general form. Their derivation did

not require assumptions of rate-limiting steps or special electric field distributions in the membrane. The rate equations have been used to further test the carrier model. In particular, the carrier's intrinsic affinities for Ca^{2+} and Sr^{2+}—K^{Ca} and K^{Sr}—were determined by two methods, the concentration dependence of *trans* acceleration and the null point determination.

Concentration Dependence of Trans Acceleration: Estimation of K^{Ca}/K^{Sr}

Trans acceleration of $^{45}Ca^{2+}$ efflux has been shown qualitatively in Figs. 3 *B* and 4 *C*. To analyze *trans* acceleration quantitatively, the initial rates of $^{45}Ca^{2+}$ efflux were

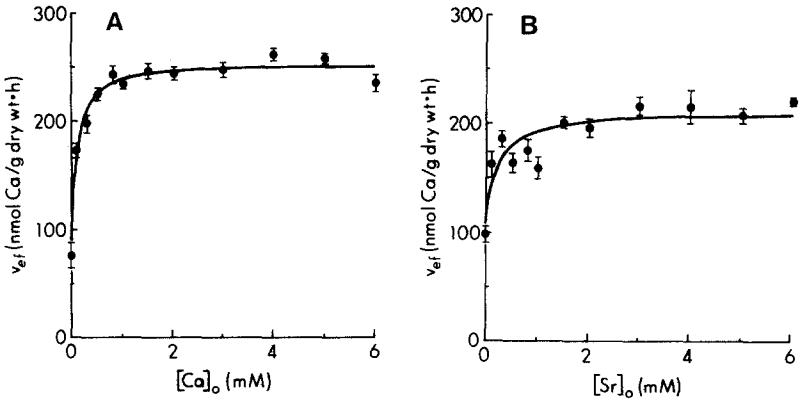

FIGURE 6. *Trans* acceleration of $^{45}Ca^{2+}$ efflux: concentration dependence. (*A*) Dependence on $[Ca^{2+}]_o$. RBCs were ATP-depleted in medium A and loaded with $^{45}Ca^{2+}$ by incubation in medium C with 1 mM $^{45}CaCl_2$ at 35°C for 53 h. $^{45}Ca^{2+}$ efflux was measured in medium C with the indicated unlabeled $[Ca^{2+}]_o$, 0.1 mM EGTA being included in the Ca^{2+}-free medium. Initial rates (using 15–18 intracellular $^{45}Ca^{2+}$ content measurements over the first 1.5 h) were determined by linear least squares. The rates (*circles*) are shown here with their estimated standard errors. The solid line represents the least-squares best fit of these rates to Eq. 3, with parameter estimates of V^{zt} = 77 ± 9 nmol/g dry wt per h, K_{1Ca} = 2,540 ± 490 nmol/g dry wt per h per mM, and K_{2Ca} = 10.0 ± 2.0 mM^{-1}. (*B*) Dependence on $[Sr^{2+}]_o$. $^{45}Ca^{2+}$ efflux from RBCs prepared as in Fig. 6 *A* was measured in medium C with the indicated unlabeled $[Sr^{2+}]_o$, 0.1 mM EGTA being included in the Sr^{2+}-free medium. Least-squares initial rates (*circles*) and their estimated standard errors are shown here with the best fit to Eq. 4, with parameter estimates of V^{zt} = 110 ± 17 nmol/g dry wt per h, exp $(2u) \times K_{1Sr}$ = 868 ± 540 nmol/g dry wt per h per mM, and K_{2Sr} = 4.06 ± 2.66 mM^{-1}. u was taken to be −0.1497 (dimensionless), based on a membrane potential of −4 mV.

measured with a range of unlabeled $[Ca^{2+}]_o$ and $[Sr^{2+}]_o$ (Fig. 6, *A* and *B*, respectively). The unidirectional rate of $^{45}Ca^{2+}$ efflux with *trans* Ca^{2+} is given by:

$$v_{ef} = \frac{V^{zt} + K_{1Ca} \times Ca_o}{1 + K_{2Ca} \times Ca_o} \tag{3}$$

where V^{zt} is the rate of efflux for zero Ca_o and K_{1Ca}/K_{2Ca} is the rate for infinite Ca_o. This

equation was derived by assuming zero $[Sr^{2+}]_i$, zero $[Sr^{2+}]_o$, and constant $[Ca^{2+}]_i$ in Eq. A2. Thus, it describes for a simple Ca^{2+} carrier how v_{ef} should vary with $[Ca^{2+}]_o$. The analogous equation for $^{45}Ca^{2+}$ efflux with *trans* $[Sr^{2+}]$, Sr_o, was derived by setting $[Ca^{2+}]_o$ and $[Sr^{2+}]_i$ equal to zero in Eq. A2 and is:

$$v_{ef} = \frac{V^{zt} + \exp(-2u) \times K_{1Sr} \times Sr_o}{1 + K_{2Sr} \times Sr_o} \tag{4}$$

Here, $\exp(-2u)$ describes the effect of a nonzero membrane potential (see Eq. A3) on the acceleration of $^{45}Ca^{2+}$ efflux by Sr^{2+}. In these equations, the five constants (V^{zt}, the two K_1's, and the two K_2's) result from regroupings of terms in Eq. A2 to define the concentration dependence of *trans* acceleration. These constants are functions of the 14 first-order rate constants in Scheme 1, the membrane potential, and $[Ca^{2+}]_i$ (which changed <20% during the measurement of initial rates). The initial efflux rates in

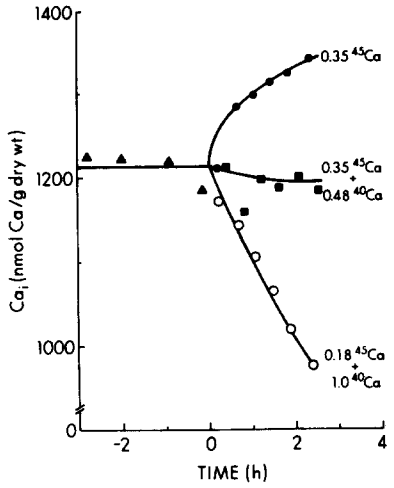

FIGURE 7. Effects of external $^{40}Ca^{2+}$ and $^{45}Ca^{2+}$ on $^{45}Ca^{2+}$ equilibrium. RBCs were ATP-depleted and loaded with $^{45}Ca^{2+}$ as described in Fig. 5. After demonstrating that the isotope was at equilibrium (*triangles*), $[^{45}Ca^{2+}]_o$ and $[^{40}Ca^{2+}]_o$ were changed to the values indicated. The inward $^{45}Ca^{2+}$ movement due to raising $[^{45}Ca^{2+}]_o$ to 0.35 mM was balanced by the outward $^{45}Ca^{2+}$ movement due to raising $[^{40}Ca^{2+}]_o$ to 0.48 mM. These values were used, along with u (Fig. 6 *B*) and an initial $[^{45}Ca^{2+}]_i$ of 0.24 mM (electrochemical equilibrium with $[^{45}Ca^{2+}]_o$ of 0.18 mM), to calculate K^{Ca} (Eq. 7).

Fig. 6, *A* and *B*, were fitted to Eqs. 3 and 4, respectively, by the unweighted least-squares method to obtain estimates for the five constants in these two equations. Using Eqs. 3, 4, and A2, the ratio of intrinsic affinities for Ca^{2+} and Sr^{2+} is given by:

$$K^{Ca}/K^{Sr} = K_{1Ca}/K_{1Sr} \tag{5}$$

Thus, using the estimates for the K_{1Ca} (Fig. 6 *A*) and K_{1Sr} (Fig. 6 *B*), K^{Ca}/K^{Sr} was 3.95. This finding is qualitatively consistent with Fig. 5, in which external unlabeled Ca^{2+} had a greater effect on $^{45}Ca^{2+}$ equilibrium than did external Sr^{2+}.

Null Point Determination of Intrinsic Affinities

The experiment shown in Fig. 7 was used to determine K^{Ca} and K^{Sr} explicitly; its design is based on changes in $[^{45}Ca^{2+}]_i$ seen after adding external labeled and unlabeled substrate to cells at $^{45}Ca^{2+}$ equilibrium. For this experiment, it is necessary

to consider the concentrations of $^{45}Ca^{2+}$ and unlabeled Ca^{2+} separately. Adding external unlabeled Ca^{2+} without changing $[^{45}Ca^{2+}]_o$ (Fig. 7, *open circles*) decreased $[^{45}Ca^{2+}]_i$, as seen previously (Fig. 5). In contrast, raising only $[^{45}Ca^{2+}]_o$ (*filled circles*) produced an increase in $[^{45}Ca^{2+}]_i$ because of carrier-mediated transport down an inward gradient. When both unlabeled Ca^{2+} and $^{45}Ca^{2+}$ are added externally, the net effect on $[^{45}Ca^{2+}]_i$ depends on the relative magnitudes of the inward and outward driving forces produced by increasing $[^{45}Ca^{2+}]_o$ and unlabeled $[Ca^{2+}]_o$, respectively. When these two forces are equal, there is no *initial* change in $[^{45}Ca^{2+}]_i$ and the unidirectional fluxes in the two directions (Eqs. A1 and A2) are equal and opposite:

$$v_{in} - v_{ef} = 0 \tag{6}$$

Combining Eqs. 6, A1, and A2, the intrinsic affinity for Ca^{2+} is:

$$K^{Ca} = \frac{^{45}Ca_o - \exp(2u) \times {}^{45}Ca_i}{^{45}Ca_i{}^{*40}Ca_o - {}^{45}Ca_o \times {}^{40}Ca_i} \tag{7}$$

where $^{45}Ca_i$, $^{45}Ca_o$, $^{40}Ca_i$, and $^{40}Ca_o$ represent the free concentrations of labeled and unlabeled Ca^{2+} on the two sides of the membrane, which result in no net movement of $^{45}Ca^{2+}$ across the membrane. This condition was satisfied by a $^{45}Ca_o$ of 0.35 mM and a $^{40}Ca_o$ of 0.48 mM (Fig. 7, *squares*). By substituting these values into Eq. 7, K^{Ca} is estimated to be 1.46 mM^{-1}. In a similar experiment where $[^{45}Ca^{2+}]_o$ and $[Sr^{2+}]_o$ were added (not shown), the estimate of K^{Sr} ranged from 0.2 to 0.5 mM^{-1}, consistent with the ratio $K^{Ca}/K^{Sr} = 3.95$, estimated by the quantification of *trans* acceleration above. Using that ratio, the best estimate for K^{Sr} is $\simeq K^{Ca}/3.95 = 0.37$ mM^{-1}.

DISCUSSION

We examined the rate and mechanism of passive Ca^{2+} movement across the human RBC membrane. Although others have examined passive Ca^{2+} entry (Ferreira and Lew, 1977; Varecka and Carafoli, 1982; Tiffert et al., 1984; McNamara and Wiley, 1986; Varecka et al., 1986), their accumulation measurements were offset by residual Ca^{2+} pump activity. These previous workers did not use ATP depletion and vanadate pretreatment simultaneously and thus did not completely inactivate the pump (Fig. 1). Because of an incompletely blocked Ca^{2+} pump, their estimates for the physiologic rate of Ca^{2+} entry, 2–20 μmol/liter cells per h, failed to match the accepted rate of active extrusion by the Ca^{2+} pump, 45 μmol/liter cells per h (Lew et al., 1982). Finally, the apparent saturability they observed is ambiguous: a nonsaturating leak offset by residual Ca^{2+} pump activity could also produce net saturable entry.

The findings of Lew et al. (1982) deserve special consideration. They found an entry rate of 48 μmol/liter cells per h into chelator-loaded RBCs in autologous plasma. This value matches their measured rate of extrusion, 45 μmol/liter cells per h. Nevertheless, in physiological saline they found a rate of only 17 μmol/liter cells per h with ATP-depleted, chelator-loaded cells (Fig. 3 of Lew et al., 1982). Our Fig. 1 *B* demonstrates that 2.5 mM vanadate must also be added to completely inhibit the Ca^{2+} pump in saline. Had they included vanadate in their experiment, the influx would have been approximately threefold greater and would have matched the

pump-mediated extrusion rate. These results suggest that there might be an endogenous Ca^{2+} pump inhibitor in plasma; this possibility warrants further study.

In saline, Ca^{2+} pump activity remains even when $[ATP]_i$ is reduced to <2 μM by ATP depletion (Ferreira and Lew, 1977). We, therefore, added vanadate to completely inactivate the Ca^{2+} pump (Fig. 1, *A* and *B*). Under these conditions, passive Ca^{2+} entry was mediated almost exclusively by a simple carrier. Its rate (53 μmol/liter cells per h) then matches the rate of active extrusion under physiologic conditions.

Competitive inhibition by *cis* Sr^{2+} (Fig. 4, *A* and *B*) and acceleration by *trans* Sr^{2+} (Fig. 4 *C*) indicate that the carrier can also transport Sr^{2+}. Two other group II divalent cations, Mg^{2+} and Ba^{2+}, were less effective in their ability to competitively inhibit and *trans* accelerate $^{45}Ca^{2+}$ movement (data not shown). Mg^{2+} was a particularly poor substrate for the carrier, consistent with the biological need to discriminate between Ca^{2+} and Mg^{2+} (Williams, 1980). Furthermore, if Mg^{2+} were a good substrate, the large inward Ca^{2+} gradient established by the Ca^{2+} pump would drive Mg^{2+} extrusion by the carrier. Because of the extremely low permeability of the RBC membrane to Mg^{2+} (Ginsburg et al., 1962), this would reduce $[Mg^{2+}]_i$ from its near-equilibrium value of 0.4 mM (Flatman and Lew, 1980) to levels much lower than needed for several critical enzymes (Wacker, 1969; Flatman and Lew, 1981).

The observed acceleration of passive $^{45}Ca^{2+}$ transport by *trans* Ca^{2+} and *trans* Sr^{2+} (Figs. 3, *A* and *B*, and 4 *C*) suggests a simple carrier (Scheme 1). This model was tested quantitatively by determining the intrinsic affinities, K^{Ca} and K^{Sr}. These constants weight all substrate concentrations appearing in the rate equations, Eqs. A1 and A2, and are thus the best indicators of the carrier's substrate preference. Also, because of their ubiquitous appearance in Eqs. A1 and A2, the intrinsic affinities are determinable by more than one experimental approach. We were technically able to apply two approaches, the *trans* substrate concentration dependence and the null point methods. Similar values for K^{Ca}/K^{Sr} were obtained by both methods, strongly supporting the simple carrier model (Stein, 1986). The relative magnitudes of K^{Ca} and K^{Sr} indicate that Ca^{2+} is the preferred substrate by fourfold (Figs. 5–7).

Other carriers such as the Cl^-/HCO_3^- (Kaplan et al., 1983; Fröhlich, 1984) and Na^+/H^+ (Aronson, 1985) exchangers function primarily as one-for-one exchangers with only rare slippage events. Indeed, those carriers may be able to release transported substrate only after binding the next substrate molecule, inconsistent with the model in Scheme 1. This would minimize slippage by disallowing the unloaded carrier forms, E_o and E_i (Stein, 1986). In contrast, the carrier described here exhibits substantial conductive Ca^{2+} flux due to slippage (Fig. 1, *A* and *B*) as well as Ca^{2+}–Ca^{2+} exchange (in cells loaded with 0.24 mM Ca^{2+}; Fig. 5). Under physiologic conditions, the extremely low $[Ca^{2+}]_i$, 20–30 nM (estimated in Lew et al., 1982), does not permit an exchange-only reaction cycle (compare the $[Ca^{2+}]_i$ of 20–30 nM to the carrier's intrinsic dissociation constant, $1/K^{Ca}$, of 0.68 mM). If physiologic Ca^{2+}–Ca^{2+} exchange were substantial, lowering $[Ca^{2+}]_i$ would be expected to reduce $^{45}Ca^{2+}$ influx. We found that exchange is negligible: subphysiologic $[Ca^{2+}]_i$ (produced by chelator loading) did not reduce $^{45}Ca^{2+}$ influx (Fig. 1 *B*). Thus, the carrier's physiologic mode of operation is net entry with almost no exchange.

APPENDIX

Unidirectional Flux Equations for the Simple Carrier of Scheme 1

The most general Ca^{2+} flux equations for the carrier in Scheme 1 are:

$$v_{in}^{s} = \frac{\overline{S}_1 + \exp(z_s u)\overline{S}_1\overline{S}_2 + \overline{S}_1\overline{P}_2}{\{R_{00} + R_{12}^{s}\overline{S}_1 + \exp(z_s u)R_{21}^{s}\overline{S}_2 + \exp(-z_p u)R_{12}^{p}\overline{P}_1 + R_{21}^{p}\overline{P}_2 + R_{ee}^{sp}\overline{S}_1\overline{P}_2 + \exp[(z_s - z_p)u]R_{ee}^{ps}\overline{S}_2\overline{P}_1 + \exp(z_s u)R_{ee}^{s}\overline{S}_1\overline{S}_2 + \exp(-z_p u)R_{ee}^{p}\overline{P}_1\overline{P}_2\}} \quad \text{(A1)}$$

$$v_{ef}^{s} = \frac{\exp(z_s u)\overline{S}_2 + \exp(z_s u)\overline{S}_1\overline{S}_2 + \exp[(z_s - z_p)u]\overline{S}_2\overline{P}_1}{\{R_{00} + R_{12}^{s}\overline{S}_1 + \exp(z_s u)R_{21}^{s}\overline{S}_2 + \exp(-z_p u)R_{12}^{p}\overline{P}_1 + R_{21}^{p}\overline{P}_2 + R_{ee}^{sp}\overline{S}_1\overline{P}_2 + \exp[(z_s - z_p)u]R_{ee}^{ps}\overline{S}_2\overline{P}_1 + \exp(z_s u)R_{ee}^{s}\overline{S}_1\overline{S}_2 + \exp(-z_p u)R_{ee}^{p}\overline{P}_1\overline{P}_2\}} \quad \text{(A2)}$$

where

$$\overline{S}_1 = K^{Ca}[Ca^{2+}]_o, \qquad \overline{S}_2 = K^{Ca}[Ca^{2+}]_i$$
$$\overline{P}_1 = K^{Sr}[Sr^{2+}]_o, \qquad \overline{P}_2 = K^{Sr}[Sr^{2+}]_i$$

K^{Ca} and K^{Sr} carrier's intrinsic affinities for Ca^{2+} and Sr^{2+}

TABLE I

Expressions for the Observable Parameters in Eqs. A1 and A2

Parameter	Expression
K^{s}	$\frac{f_1 f_2 g_1}{f_2 g_1 k_1 + f_1 g_1 k_2 \exp(z_s u) + b_1 f_2 k_1}$
K^{p}	$\frac{e_1 e_2 h_2}{e_1 h_2 k_2 + e_2 h_2 k_1 \exp(-z_p u) + d_2 e_1 k_2}$
$E_{tot} \times R_{00}$	$\frac{1}{k_1} + \frac{1}{k_2}$
$E_{tot} \times R_{12}^{s}$	$\frac{1}{b_2} + \frac{1}{g_1} + \frac{1}{k_2} + \frac{g_2}{b_2 g_1}$
$E_{tot} \times R_{21}^{s}$	$\frac{1}{b_1} + \frac{1}{g_2} + \frac{1}{k_1} + \frac{g_1}{b_1 g_2}$
$E_{tot} \times R_{12}^{p}$	$\frac{1}{d_2} + \frac{1}{h_1} + \frac{1}{k_2} + \frac{h_2}{d_2 h_1}$
$E_{tot} \times R_{21}^{p}$	$\frac{1}{d_1} + \frac{1}{h_2} + \frac{1}{k_1} + \frac{h_1}{d_1 h_2}$
$E_{tot} \times R_{ee}^{sp}$	$\frac{1}{b_2} + \frac{1}{d_1} + \frac{1}{g_1} + \frac{1}{h_2} + \frac{g_2}{b_2 g_1} + \frac{h_1}{d_1 h_2}$
$E_{tot} \times R_{ee}^{ps}$	$\frac{1}{b_1} + \frac{1}{d_2} + \frac{1}{g_2} + \frac{1}{h_1} + \frac{g_1}{b_1 g_2} + \frac{h_2}{d_2 h_1}$
$E_{tot} \times R_{ee}^{s}$	$\frac{1}{b_1} + \frac{1}{b_2} + \frac{1}{g_1} + \frac{1}{g_2} + \frac{g_1}{b_1 g_2} + \frac{g_2}{b_2 g_1}$
$E_{tot} \times R_{ee}^{p}$	$\frac{1}{d_1} + \frac{1}{d_2} + \frac{1}{h_1} + \frac{1}{h_2} + \frac{h_1}{d_1 h_2} + \frac{h_2}{d_2 h_1}$

The parameters in Eqs. A1 and A2 are obtained by regrouping terms in the derived unidirectional rate equations according to substrate concentrations. These are represented here by a notation similar to that suggested by Stein (1986). E_{tot} represents the total concentration of the carrier (sum of all six forms in Scheme 1).

R (with subscripts) resistance terms describing ease of interconversion between carrier intermediates (notation of Stein, 1986)

z_s and z_p valences of S and P (Ca^{2+} and Sr^{2+}, respectively)

and

$$u = FV_m/RT$$

where

F the Faraday

V_m membrane potential

R (no subscript) the gas constant

T absolute temperature

The resistance terms (R's with subscripts), K^{Ca}, and K^{Sr} are functions of the 14 first-order rate constants in Scheme 1, z_s and z_p, and u, but *not* of the concentrations of S or P. These functions are given explicitly in Table I.

We thank Dr. Paul De Weer and Dr. Albert Roos for their help and advice.

These studies were supported by grant HL-12839 from the National Heart, Lung and Blood Institute, grant AI-07172 from the National Institute of Allergy and Infectious Diseases, and grant GMO-7200 from the National Institute of General Medical Sciences.

Original version received 9 July 1990 and accepted version received 4 January 1991.

REFERENCES

Aronson, P. S. 1985. Kinetic properties of the plasma membrane Na^+-H^+ exchanger. *Annual Review of Physiology.* 47:545–560.

Bond, G. H., and P. M. Hudgins. 1978. Kinetics of inhibition of red cell membrane Ca-ATPase by pentavalent vanadium. *Federation Proceedings.* 37:313. (Abstr.)

Cantley, L. C., M. D. Resh, and G. Guidotti. 1978. Vanadate inhibits the red cell (Na^+, K^+) ATPase from the cytoplasmic side. *Nature.* 272:552–554.

Carafoli, E. 1987. Intracellular calcium homeostasis. *Annual Review of Biochemistry.* 56:395–433.

De Weer, P., and A. G. Lowe. 1973. Myokinase equilibrium. An enzymatic method for the determination of stability constants of magnesium complexes with adenosine triphosphate, adenosine diphosphate, and adenosine monophosphate in media of high ionic strength. *Journal of Biological Chemistry.* 248:2829–2835.

Draper, N. R., and H. Smith. 1981. Applied Regression Analysis. John Wiley & Sons, Inc., New York. 407 pp.

Ferreira, H. G., and V. L. Lew. 1977. Passive Ca transport and cytoplasmic Ca buffering in intact red cells. *In* Membrane Transport in Red Cells. J. C. Ellory and V. L. Lew, editors. Academic Press, New York. 53–91.

Flatman, P. W., and V. L. Lew. 1980. Magnesium buffering in intact human red blood cells measured using the ionophore A23187. *Journal of Physiology.* 305:13–30.

Flatman, P. W., and V. L. Lew. 1981. The magnesium dependence of sodium-pump-mediated sodium-potassium and sodium-sodium exchange in intact human red cells. *Journal of Physiology.* 315:421–446.

Freedman, J. C., and J. F. Hoffman. 1979. Ionic and osmotic equilibria of human red blood cells treated with nystatin. *Journal of General Physiology.* 74:157–185.

Fröhlich, O. 1984. Relative contributions of the slippage and tunneling mechanisms to anion net efflux from human erythrocytes. *Journal of General Physiology.* 84:877–893.

Ginsburg, S., J. G. Smith, F. M. Ginsburg, J. Z. Reardon, and J. K. Aikawa. 1962. Magnesium metabolism of human and rabbit erythrocytes. *Blood.* 20:722–729.

Kaplan, J. H., M. Pring, and H. Passow. 1983. Band-3 protein-mediated anion conductance of the red cell membrane: slippage vs. ionic diffusion. *FEBS Letters.* 156:175–179.

Läuger, P. 1980. Kinetic properties of ion carriers and channels. *Journal of Membrane Biology.* 57:163–178.

Lew, V. L. 1971. On the ATP dependence of the Ca^{2+}-induced increase in K^+ permeability observed in human red cells. *Biochimica et Biophysica Acta.* 233:827–830.

Lew, V. L., R. Y. Tsien, C. Miner, and R. M. Bookchin. 1982. Physiological $[Ca^{2+}]_i$ level and pump-leak turnover in intact red cells measured using an incorporated Ca chelator. *Nature.* 298:478–481.

Lieb, W. R. 1982. A kinetic approach to transport studies. *In* Red Cell Membranes: A Methodological Approach. J. C. Ellory and J. D. Young, editors. Academic Press, London. 135–164.

McNamara, M. K., and J. S. Wiley. 1986. Passive permeability of human red blood cells to calcium. *American Journal of Physiology.* 250:C26–C31.

Niggli, V., E. S. Adunyah, J. T. Penniston, and E. Carafoli. 1981. Purified (Ca^{2+}-Mg^{2+})-ATPase of the erythrocyte membrane. Reconstitution and effect of calmodulin and phospholipids. *Journal of Biological Chemistry.* 256:395–401.

Schatzmann, H. J. 1985. Calcium extrusion across the plasma membrane by the calcium-pump and the Ca^{2+}-Na^+ exchange system. *In* Calcium and Cell Physiology. D. Marmé, editor. Springer-Verlag, Berlin. 18–52.

Simonsen, L. O. 1980. Binding of ionophore A23187 by bovine plasma albumin. *Journal of Physiology.* 313:34P–35P. (Abstr.)

Stein, W. D. 1986. Transport and Diffusion across Cell Membranes. Academic Press, Orlando, FL. 685 pp.

Tiffert, T., J. Garcia-Sancho, and V. L. Lew. 1984. Irreversible ATP depletion caused by low concentrations of formaldehyde and of calcium-chelator esters in intact human red cells. *Biochimica et Biophysica Acta.* 773:143–156.

Tsien, R. Y. 1981. A non-disruptive technique for loading calciun. buffers and indicators into cells. *Nature.* 290:527–528.

Varecka, L., and E. Carafoli. 1982. Vanadate-induced movements of Ca^{2+} and K^+ in human red blood cells. *Journal of Biological Chemistry.* 257:7414–7421.

Varecka, L., E. Peterajová, and J. Pogády. 1986. Inhibition by divalent cations and sulphydryl reagents of the passive Ca^{2+} transport in human red blood cells observed in the presence of vanadate. *Biochimica et Biophysica Acta.* 856:585–594.

Wacker, W. E. C. 1969. The biochemistry of magnesium. *Annals of the New York Academy of Sciences.* 162:717–726.

Weith, J. O., J. Funder, R. B. Gunn, and J. Brahm. 1974. Passive transport pathways for chloride and urea through the red cell membrane. *In* Comparative Biochemistry and Physiology of Transport. L. Bolis, K. Bloch, S. E. Luria, and F. Lynen, editors. North-Holland Publishing Company, Amsterdam. 317–337.

Williams, R. J. P. 1980. A general introduction to the special properties of the calcium ion and their deployment in biology. *In* Calcium-binding proteins: Structure and Function. F. Siegal, E. Carafoli, R. Kretsinger, D. MacLennan, and R. Wasserman, editors. Elsevier North Holland, New York, 3–10.